Journal Pre-proofs

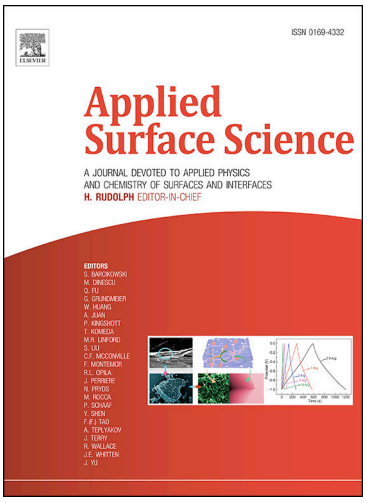

Full Length Article

Reactivity passivation of red phosphorus with thin plasma-deposited carbon coating

Paige C. Kinsley, Aiping Zeng, Jenny K. Hedlund Orbeck, Shaun Debow, Zachary B. Zander, Patrick J. Heaney, Robert J. Hamers

PII: S0169-4332(22)00369-5
DOI: https://doi.org/10.1016/j.apsusc.2022.152791
Reference: APSUSC 152791

To appear in: *Applied Surface Science*

Received Date: 5 December 2021
Revised Date: 31 January 2022
Accepted Date: 7 February 2022

Please cite this article as: P.C. Kinsley, A. Zeng, J.K. Hedlund Orbeck, S. Debow, Z.B. Zander, P.J. Heaney, R.J. Hamers, Reactivity passivation of red phosphorus with thin plasma-deposited carbon coating, *Applied Surface Science* (2022), doi: https://doi.org/10.1016/j.apsusc.2022.152791

Title: Reactivity passivation of red phosphorus with thin plasma-deposited carbon coating

Authors: Paige C. Kinsley[a], Aiping Zeng[b], Jenny K. Hedlund Orbeck[a], Shaun Debow[c], Zachary B. Zander[c], Patrick J. Heaney[b], Robert J. Hamers[a*]

Institutions:

[a]University of Wisconsin-Madison, 1101 University Avenue, Madison, WI 53706, USA

[b]NCD Technologies, 510 Charmany Drive, Suite 258, Madison, WI 53719, USA

[c]U.S. Army Combat Capabilities Development Command Chemical Biological Center, Research & Technology Directorate, 8198 Blackhawk Rd, Aberdeen Proving Ground, MD 21010, USA

*Corresponding Author: Robert Hamers (rjhamers@wisc.edu)

Abstract

Red phosphorus, when exposed to humid environments in air, breaks down into toxic phosphine gas and acidic phosphorus species, presenting a challenge for many applications, such as flame retardants or pyrotechnic obscurants. We have developed and characterized a method of plasma-deposited carbon to form a nanometer-thick, chemically stable carbon layer on red phosphorus particles to suppress phosphine and acidic phosphorus production. Using a combination of XPS surface analysis and a novel IR headspace analysis method, we developed and quantified an understanding of the reaction of red phosphorus with water vapor and the suppression of decomposition products using plasma-deposited carbon coatings. Phosphine production, quantified by IR, was accompanied by the formation of surface PO_x species produced as the particles react with water vapor. Increasing plasma deposition time increased thickness and uniformity of graphitic carbon coating, corresponding to a marked decrease in phosphine generation and formation of surface PO_x species.

Graphical abstract

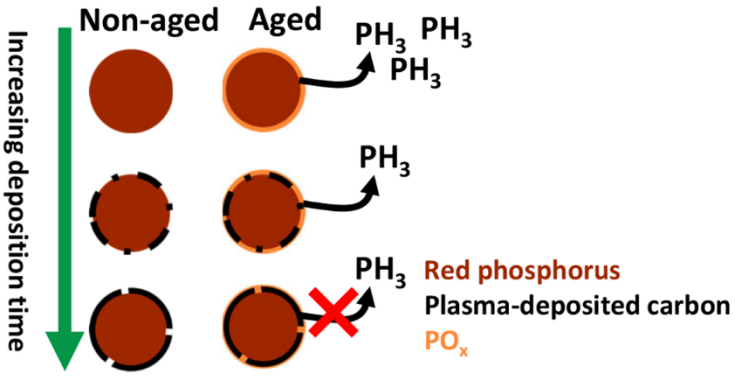

Keywords: Phosphorus; Surface reaction; X-ray photoelectron spectroscopy; Infrared spectroscopy; Infrared head-space analysis; Phosphine

1. Introduction

Red phosphorus (RP) is a phosphorus allotrope commonly used as a flame retardant in thermoplastics and as an obscurant to attenuate transmission in visible and IR regions in military applications [1]. It has also been used in composites for anodes for sodium ion batteries [2]. While its chemical properties make it well suited for these applications, its reactivity with water and oxygen is an obstacle for safe use. When red phosphorus reacts with water, it evolves phosphine (PH_3), a highly toxic gas even at low levels, and acidic phosphorus species, primarily phosphoric and phosphorous acids [3-5]. Formation and accumulation of phosphine due to storage conditions of red phosphorus can potentially lead to human health hazards because of the high toxicity of phosphine. Further decomposition can form phosphorous and phosphoric acids on surfaces, leading to corrosion and failure of components or electronic connections [6-8]. To mitigate degradation of red phosphorus, some manufacturers have added in components that sequester phosphine as it is generated or neutralizes acid species using alkaline compounds [1, 9, 10]. Alternatively, red phosphorus can be mixed with amides and ester-based polymers to protect the surface of the phosphorus particles from direct contact with water or air. However, these polymer coatings are less effective at suppressing phosphine formation at elevated temperatures. Furthermore, phosphorus must be burned when used as a smoke obscurant, and these coatings produce toxic carbon-based byproducts under these conditions. [1, 11]. Additionally, many

additives require a high additive-to-red-phosphorus ratio to be effective, decreasing the amount of active species by mass.

An alternative approach to mitigating the reactivity of phosphorus is coating the individual phosphorus particles with a thin protective layer, forming a core-shell structure. Carbon coatings are chemically and thermally stable [12] and have been successfully used in the battery industry as a way to improve electrical properties for active anode and cathode powders, reducing reactivity with liquid electrolytes [13]. Additionally, we predict these thin carbon coatings will not impact desired red phosphorus combustion properties because of their small heat capacity compared to polymer counterparts. While carbon coatings can be applied using several approaches [14-16], plasma deposition methods can be applied to both planar and powder samples and can be scaled up to kilogram ranges [17, 18]. The resulting layers can be conformal, with controlled thickness and are typically hydrophobic, thereby resisting entrapment of water in powdered samples.

Here, we report an investigation of the surface transformations of red phosphorus with water vapor. Using a combination of gas-phase infrared spectroscopy (IR) and x-ray photoelectron spectroscopy (XPS), we demonstrate the ability to characterize and quantify red phosphorus transformation as it ages, as well as the impact of plasma-deposited carbon surface coatings on the transformation. Tracking PH_3 generation by IR and oxidized phosphorus species production by XPS and IR, we gain insight into how RP degrades as it ages in humid environments. This study provides insight into the efficacy of plasma-deposited carbon on passivation of RP as well as building a picture of the mechanism of RP degradation.

2. Materials and methods

2.1. *Materials*

Red phosphorus (Manufacturer: <100 μm, 98%, MIL DTL 211 F Class 4) was purchased from Italmatch Chemicals. Zinc sulfide (10 μm, 99.99% trace metals basis), zinc phosphide (≥19% active phoshor (P) basis, powder), sodium hydroxide (ACS reagent, ≥97.0%, pellets), and hydrochloric acid (ACS reagent, 37%) were all purchased from Sigma Aldrich. Acetylene (99.6%) was purchased from Airgas. Aging conditions for red phosphorus and titrations were done using ultrapure water (18.2 MΩ).

2.2. *Red phosphorus preparation and plasma-deposited carbon (PDC) coating*

Red phosphorus particles were cleaned and coated using a plasma source ion immersion implantation and deposition process with a pulsed DC power supply. The apparatus used for carbon coating is similar to deposition systems reported previously. [19, 20]. Specifically, we employed a rotating cathodic plasma tank installed at NCD Technologies. The RP particles were first dried in vacuum to remove adsorbed moisture, and then cleaned using an argon/hydrogen plasma followed by an argon plasma. Following plasma cleaning, cathodic plasma tank parameters are adjusted to deposit a carbon coating on the RP particles using an acetylene precursor gas. The plasma tank design allows for ball milling during plasma cleaning and carbon deposition to further separate RP clumps and reduce particle size to avoid particle aggregation during carbon deposition. The PDC deposition times were 0, 4, 8, and 24 min/g, where the exposure to the plasma was normalized by the mass of RP sample in the reactor to help compensate for differences in surface coverage due to slightly varying amounts of phosphorus. Samples will be referred to RP-uncoated (0 min/g) and for coated red phosphorus, RP@C-short (4 min/g), RP@C-medium (8 min/g), and RP@C-long (24 min/g) throughout the paper. Specifics on flow rate and reactor set up can be found in a patent soon to be published.

2.3. *Characterization of non-aged red phosphorus particles*

Scanning electron microscopy (SEM) measurements were taken on a Leo Supra55 VP SEM at 1 kV using a secondary electron detector. SEM samples were prepared by making a red phosphorus and isopropyl alcohol solution that was then drop-cast on a boron-doped silicon wafer. To prepare samples for surface area characterization using Brunauer-Emmet-Teller (BET) analysis, ~170 mg of sample was weighed and degassed at 120°C for 2 hours under vacuum. Samples were analyzed using a Micrometrics Gemeni VII 2390 surface analyzer, measuring nitrogen absorption isotherms. BET analysis gave an average particle size on the order of several microns, and SEM showed a broad distribution of sizes. Raman measurements were taken using a Thermo-Fischer Scientific DXRxi Raman imaging microscope using 532 nm laser excitation at 2 mW power and 10x objective. Samples were prepared as described in section 2.6 (using the same preparation as XPS samples).

2.4. *Gas-phase infrared spectroscopy*

Gas-phase infrared (IR) spectra were collected using a Bruker Vertex 70 spectrometer at a resolution of 0.5 cm^{-1} and collected from 5000 to 700 cm^{-1}, with 100 scans per spectrum. Spectra were collected in a transmission geometry with a 10 cm path length (see SI Figure 1 for gas phase IR cell dimensions). For each phosphine generation experiment, 0.500 g of red phosphorus was added to one sample bulb (SI Figure 1b) and 1.000 mL of nanopure water to the other. After sealing bulbs onto cell with vacuum grease and parafilm, a 0-hour baseline spectrum was taken for each sample using the above instrument parameters. The cells were then stored in an incubator at 50°C between time points. To prevent accumulation of water condensation on the red phosphorus particles, the cells were stored in a custom-made aluminum holder and tilted at an angle (see SI Figure 1c). Three replicates for each sample were measured for statistical analysis.

For experimental phosphine calibration of IR instrument, zinc phosphide powder was dissolved in 5N hydrochloric acid to produce pure phosphine gas. A gas tube, filled with HCl and capped with a septum, was used to collect PH_3 bubbles produced by dissolving zinc phosphide. A known volume of PH_3 was collected by syringe and transferred to a septum-capped gas phase IR cell filled with air at atmosphere. Spectra were measured using the same instrument parameters as gas-phase IR PH_3 experiments with red phosphorus.

2.5. *Diffuse reflectance infrared spectroscopy*

Diffuse reflectance infrared spectroscopy (DRIFTS) spectra were collected using a Bruker Vertex 70 at a resolution of 4 cm^{-1} and collected between 5000 to 700 cm^{-1}, with 500 scans collected each spectrum. Uncoated red phosphorus was mixed with dry zinc sulfide at a 1:100 mass ratio and placed in to a Praying Mantis™ High Temperature Reaction Chamber, which provides a hermetically sealed environment for gas-solid interactions. The RP/ZnS sample was added to the chamber along with 0.800 mL of nanopure water, and the chamber was then sealed. After taking a spectrum at 0 hours, the reaction chamber was stored at 50°C for 24 hours and another spectrum was taken for comparison.

2.6. *X-ray photoelectron spectroscopy*

X-ray photoelectron spectroscopy (XPS) data were obtained on a Thermo K-alpha XPS using an Al Kα source (1486.6 eV photon energy) at a 45° take-off angle. Survey spectra were taken at a

pass energy of 200 eV and resolution of 1 eV/step. For the C(1s), P(2p), and O(1s) peaks, we used a 50 eV pass energy and 0.200 eV/step resolution. Data were analyzed using CasaXPS; peak-fitting was performed using a Shirley background fit and a GL(30) mixed Gaussian-Lorentzian line shape [21]. All energies were calibrated to the 284.8 eV binding energy of adventitious carbon [22].

Samples were prepared by pressing sample powder into indium foil mounted on a copper substrate. To remove any residual moisture, aged samples from gas-phase IR experiments were first dried in a vacuum oven at 35°C for 2 hours before pressing. Three replicates were taken for statistical analysis, with three points taken per replicate.

To calculate the carbon thickness for each deposition rate, we used a model that includes the influence of electron scattering within the phosphorus and within the graphite layer, as reported previously [23].

$$\frac{1-e^{-t_c/\lambda_{C1s,graphite}}}{e^{-t_c/\lambda_{P2p,\,graphite}}} = \frac{Area_{C1s}}{Area_{P2p}} \cdot \frac{\rho_P}{\rho_C} \cdot \frac{SF_{P2p}}{SF_{C1s}} \cdot \frac{\lambda_{P2p,Red\,P}}{\lambda_{C1s,graphite}} \qquad (1)$$

Where t_c = carbon coating thickness in nm, *Area* = integrated peak area, ρ = density of element in atoms/nm^3 (ρ_p = 42 atoms/nm^3 for P in red phosphorus, ρ_C = 130.5 atoms/nm^3 for C in amorphous carbon [24]), *SF* = elemental sensitivity factor ($SF_{P(2p)}$ = 1.3529, $SF_{C(1s)}$ = 1), $\lambda_{A,B}$ represents the inelastic mean free path of electrons "A" through the material "B". We used $\lambda_{P2p,\,Red\,P}$ = 2.90 nm, $\lambda_{P2p,\,graphite}$ = 1.99 nm, and $\lambda_{C1s,\,graphite}$ = 1.81 nm (based on calculations using the NIST Electron Inelastic-Mean-Free-Path Database [25]). This equation cannot be solved analytically but can be solved numerically or graphically to determine the carbon layer thickness t_c [26].

The atomic percent of specific species in the region probed by XPS was calculated using the following equation:

$$Atomic\ \% = 100 * \frac{\frac{Area_A}{N_A SF_A}}{\frac{Area_A}{N_A SF_A} + \frac{Area_B}{N_B SF_B}} \quad (3)$$

Where *Area* = integrated peak area, *SF* = elemental sensitivity factor ($SF_{P(2p)}$ = 1.3529, $SF_{C(1s)}$ = 1) and *N* = number of summed sweeps acquired for a specific element.

To calculate the percent oxidized phosphorus composition based on P(2p) emission intensity, we used equation 4:

$$PO_x\%\ of\ P(2p) = \frac{Area_{PO4}}{Area_{PO4} + Area_{Elemental\ P,corrected}} * 100 \quad (4)$$

See Supplementary Material for equation and explanation for corrected elemental P area in equation 4.

2.7. *Acid-base titration*

To quantify the acid species adsorbed to the surface of red phosphorus particles after aging for gas-phase IR data collection, each RP specimen was suspended in its corresponding 1.000 mL of water used in the gas-phase IR experimental methods section (from the water bulb in SI Figure 1) and centrifuged at 14,500x rpm for 5 min. The supernatant was then taken, diluted to 10.0 mL, and titrated with 37.60 mL of 0.0100 M NaOH to determine the identity and concentration of phosphorus acid species.

3. Results and discussion

3.1. *Influence of carbon coating on particle properties*

Before testing the efficacy of the carbon coating on the suppression of red phosphorus transformations, we characterized the effect of carbon deposition time on carbon composition and coverage. Increasing carbon deposition affected both the size and surface area of the particles. SI Figure 2 shows increasing deposition time corresponds to an increase in surface area, as measured by BET surface area analysis. Specifically, the surface area of the particles

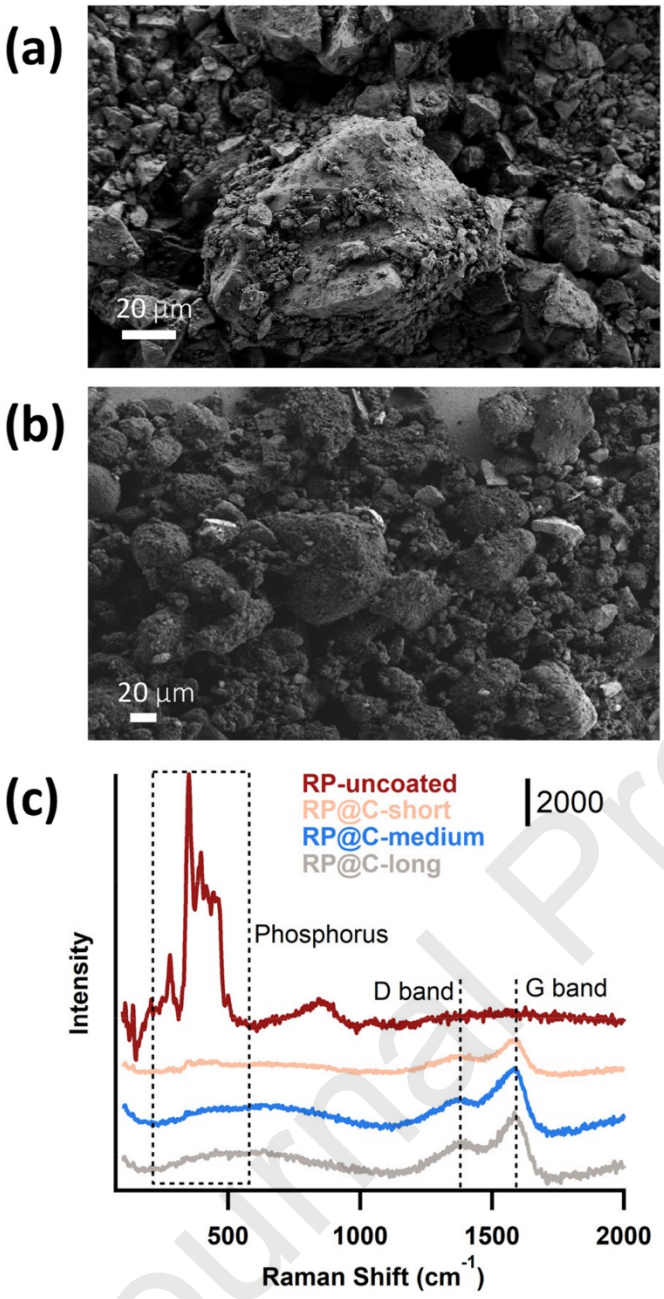

Figure 1. SEM micrographs of (a) non-aged uncoated red phosphorus and (b) RP@C-long and (c) Raman spectra for non-aged red phosphorus with various carbon deposition times.

increased 10-fold from uncoated particles (0 min) compared with particles coated for the longest deposition time, at 24 min. To understand the origin of this increase, particles were imaged using scanning electron microscopy (Figure 1a and 1b). Because the secondary electron (SE) yield of phosphorus is greater than carbon, phosphorus appears brighter in SEM images, providing a way to distinguish between carbon and phosphorus. Based on the examination of many images, we observe that particle appearances changes with increasing deposition time. Specifically, uncoated particles appear smooth with high SE yield, while RP@C-long have a rougher surface with lower SE yield. This suggests that, with increasing deposition time, smoother phosphorus is covered with rougher carbon. Compared to the relatively smooth surface of uncoated red phosphorus, the carbon coating is rough at the submicron scale, leading to a further increase in surface area of each particle, corresponding to BET surface area analysis data.

While SEM shows that the coating appears particle-like, we used Raman to identify the nature of the carbon coating. Uncoated RP particles show strong phosphorus bands between 300-500 cm^{-1} (Figure 1c) [27]. As the duration of carbon deposition increases, the phosphorus bands at 350 cm^{-1}, 396 cm^{-1}, and 444 cm^{-1} decrease in intensity (for RP@C-short) and then disappear (for RP@C-long), while new bands arise near

1385 cm^{-1} and 1586 cm^{-1}. Bands in this region are well known and are frequently referred to as the D band and G band, respectively [28, 29]. Ferrari and Robertson introduced a three-stage model of carbon ordering (transitioning from graphite to tetrahedral amorphous carbon) based on the Raman shift of the G band the ratio of intensities I(D)/I(G) [29]. Our measurements (SI Table 1) show that regardless of PDC deposition time, the G band remains between 1585-1590 cm^{-1} and the I(D)/I(G) remains approximately 0.45. These results correspond to stage 1 carbon, indicating more graphite than nanocrystalline graphite on the surface with mostly sp^2 hybridization, and no measurable presence of amorphous carbon [29]. Characterization of the pristine carbon coating can provide insight into the passivation of the red phosphorus surface.

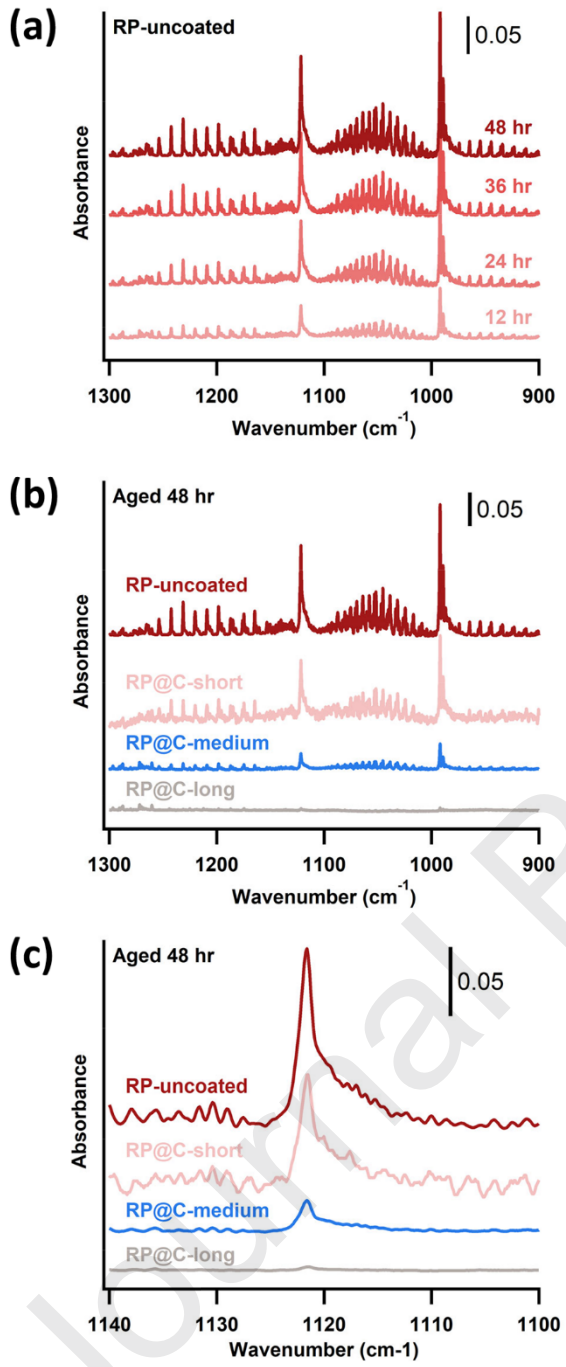

Figure 2. IR headspace spectra showing changes in PH_3 as a function of time and of RP coating. (a) Uncoated RP after exposure to H_2O vapor over 48h; (b) IR spectra for RP samples with coated at varying PDC deposition times after 48h aging at 50°C, 100% humidity, and (c) same as (b) except higher-resolution examination of the spectral region used for quantitative analysis.

We quantified PH_3 generation using infrared analysis of phosphine generated from red phosphorus samples. Two PH_3 vibrational bands are conveniently located in mid-infrared regions and do not overlap with CO_2, H_2O, or other infrared-active contaminants. The PH_3 υ_2 band is centered near 992.1 cm^{-1} and the υ_4^1 band is centered at 1118.3 cm^{-1} [30, 31]. Due to its odd number of electrons, PH_3 has allowed Q branch transitions (e.g., $\Delta J=0$), leading to a strong, slightly broad peak centered at each band head, along with sharper but weaker lines due to P ($\Delta J=-1$) and R ($\Delta J=+1$) transitions in the adjacent regions. A sealed IR cell allowed us to intentionally expose red phosphorus to high temperature, high humidity environments while safely measuring PH_3 generation over time. To establish how the amount of phosphine produced depends on aging conditions, we acquired spectra every 12 hours for 48 hours. Figure 2a shows typical phosphine spectra for uncoated RP particles aged over 48 hours. Using the linear calibration curve in SI Figure 4, we quantified the amount of PH_3 by comparing the peak intensity of the υ_4^1 band at 1118.3 cm^{-1} of the uncoated and coated red phosphorus samples, seen in Figure 2c at the 48-hour timepoint, to the

peak intensities measured for samples of dilute PH_3 gas. We further verified the validity of our calibration by comparing integrated absorption intensities of our self-generated calibrations with integrated absorbance values of individual infrared transitions at 944.4 cm^{-1}, published previously [30, 31].

To determine the impact of the plasma-deposited carbon coating on the suppression of phosphine generation, RP samples that were exposed to the plasma for increasing lengths of time were aged for 48 h (100% humidity, 50°C). Figure 2b shows the resulting spectra. Figure 2b and 2c shows that the samples exposed to the DC plasma for greater lengths of time produced less PH_3, and the sample having the longest exposure (RP@C-long) showed no detectable PH_3 generation after 48 hours of aging.

Duration of plasma deposition	Initial PH_3 production rate (Vol %/hr)	Normalized PH_3 production rate, relative to uncoated P
Uncoated	0.040 ± 0.014	1

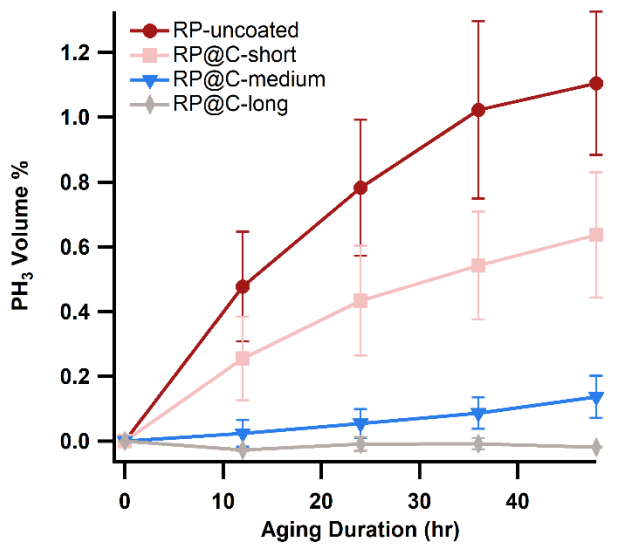

Figure 3. Cumulative production of PH_3 vs. duration of aging, for bare RP (0 min) and for samples exposed to the carbon plasma for increasing lengths of time.

Table 1. Effect of carbon deposition time on initial rate of PH_3 production from IR for first 12 hours.

We converted the IR absorbance values to PH_3 volume percent, giving the result shown in Figure 3. While the cumulative amount of PH_3 formed continually increases as the samples are aged, the rate of PH_3 formation appears to decrease at longer aging times. Table 1 shows the initial PH_3 generation rate, obtained from the initial slope between 0 and 12 hours of the data in Figure 3. With increasing deposition time, both the initial rate of PH_3 generation and the final amount of PH_3 generated are suppressed. Increasing deposition of plasma-deposited carbon coating suppresses generation of phosphine as measured by infrared spectroscopy.

3.2. *Surface analysis of non-aged red phosphorus samples*

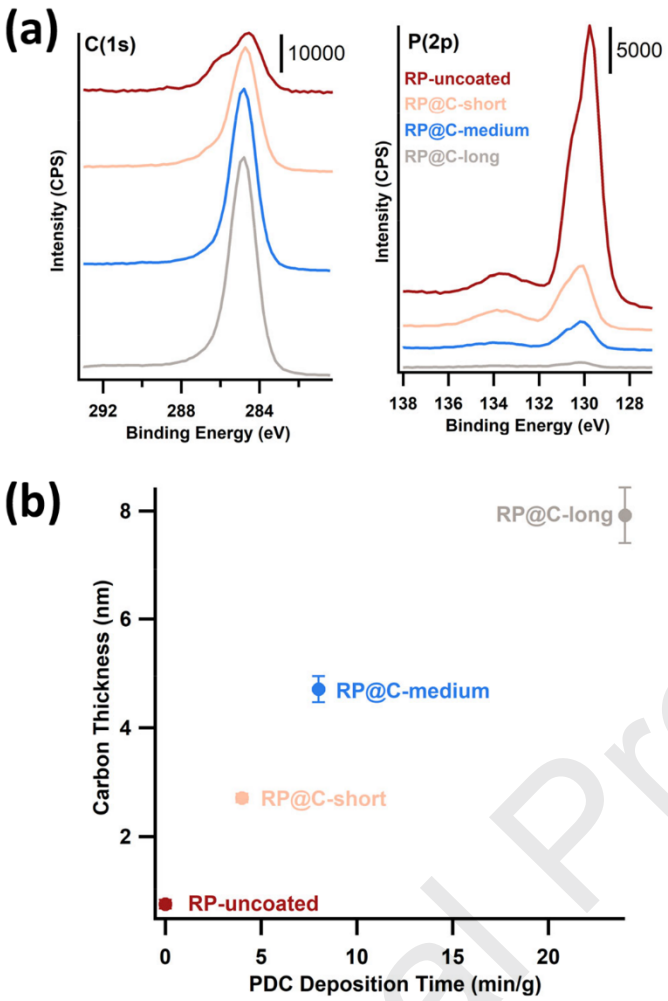

Figure 4. (a) XPS C(1s) and P(2p) intensities (in counts per second) for nonaged RP samples prepared using indicated carbon plasma deposition times and (b) thickness of carbon layer calculated from XPS attenuation data for nonaged samples.

XPS measurements provided useful information to show how RP particle surface chemistry was altered as an effect of coating and aging. Given that the phosphine generation from coated particles is significantly suppressed with the carbon coating, we first characterized the surface of non-aged particles using XPS to understand the starting surface chemistry of each sample.

Figure 4a and 4b show the effect of deposition time on C(1s) and P(2p) intensities for non-aged samples. Figure 4a shows that as the absolute intensity for C(1s) increases, the intensity of the P(2p) intensity decreases, indicating attenuation of phosphorus by a carbon coating. SI Figure 5 shows a corresponding decrease in the O(1s) and Na(1s) regions, as the cleaning and then carbon coating treatments remove sodium and oxygen species left from RP synthesis [3]. We attribute carbon present on the uncoated particles to contaminants adsorbed from the environment (frequently referred to as “adventitious carbon”). We anticipate that surface contaminants are likely removed during the plasma deposition process such that their presence on the uncoated particles should not interfere with the intentional formation of carbon coatings or subsequent measurements on carbon-coated powders. We have calculated the apparent thickness of the plasma-deposited carbon on the red phosphorus particles by applying equation 1. Figure 4b shows the carbon thickness obtained from samples exposed to the PCD for different lengths of time. These data show that a carbon coating of only

~ 8 nm thick on average can almost completely suppress the production of PH_3 based on calculated PH_3 volumes in Figure 3a. Increasing the PDC coating rate does not correspond to linear increase of apparent thickness of carbon on red phosphorus surface but does follow a trend of PH_3 suppression with increasing carbon thickness.

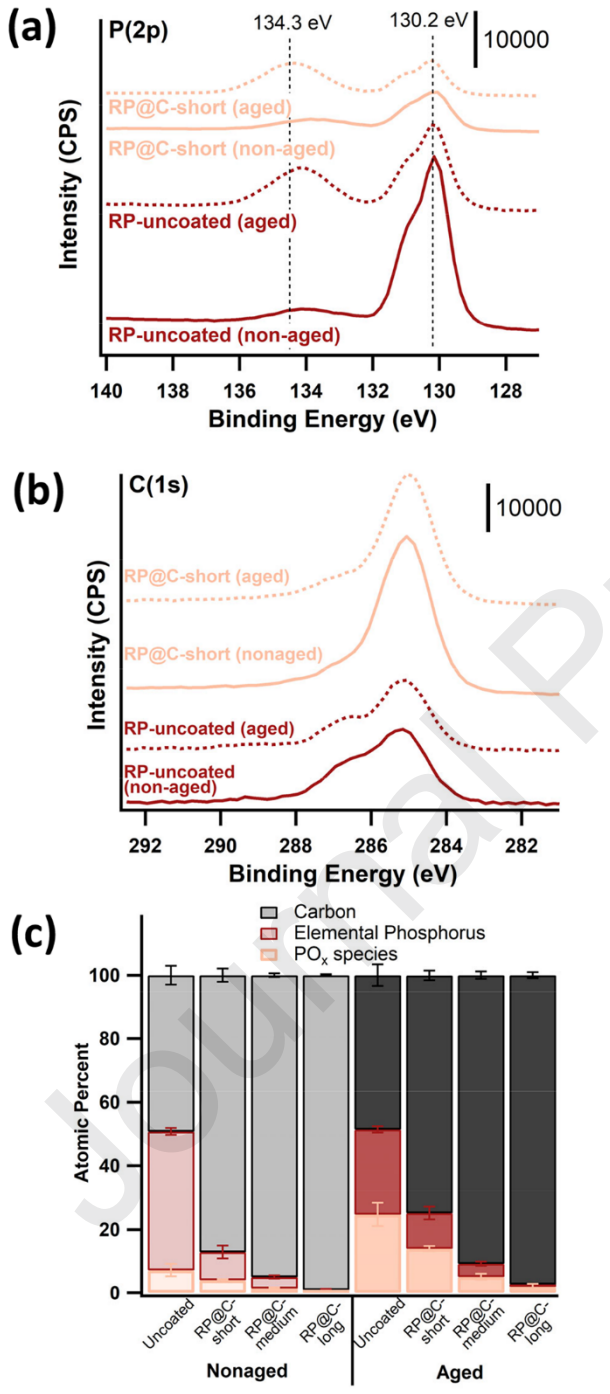

Figure 5. XPS of (a) C(1s) and (b) P(2p) intensities (in counts per second) for uncoated and RP@C-short particles before and after aging and (c) calculated atomic percent for carbon, elemental phosphorus, and oxidized phosphorus as affected by aging and carbon coating deposition time.

3.3. *Evolution of phosphorus chemical state*

Prior studies have shown that reduction of P to produce PH_3 is accompanied by oxidation to form different phosphate and phosphonate species [3]. To probe the transformations of red phosphorus after being exposed to the high humidity, high temperature conditions used for the phosphine generation IR experiments, we used XPS to probe the P(2p) region of samples aged at 50°C for 48 hours.

Figure 5a and 5b show the changes in the P(2p) and C(1s) regions as an effect of 48 hours of aging for uncoated particles and particles coated over the "short" time period (RP@C-short). The P(2p) region shows that before aging, the elemental P peak (130.2 eV) is larger for uncoated RP. After aging for 48 hours, the elemental peak decreases, while the peak corresponding to oxidized phosphorus species at 134.3 eV grows for both samples. Figure 5b shows a decrease in the C(1s) peak height for both uncoated and coated particles after aging.

To quantify these changes in relative species abundance, we used equation 3 to calculate the atomic percentage of the probed region for carbon, elemental phosphorus, and oxidized phosphorus (PO_x species). Figure 5c shows the changes in the atomic percent of each species as a function of deposition time for both non-aged and aged red phosphorus particles. Focusing first on non-aged samples, we see the surface composition increase from roughly 50% carbon on uncoated particles to 99.0±0.3% for particles coated for the longest period of time. The increase in carbon corresponds to a decrease in phosphorus, which is mostly made up of elemental P species for non-aged samples regardless of carbon deposition time. After aging, the atomic percent of carbon decreases for all samples, but most substantially for RP@C-short, decreasing from 87.1±2.1%C to 74.8±1.5%C (all values presented in SI Table 2). The decrease in atomic percent of carbon corresponds to only a slight increase in elemental phosphorus signal but a significant increase in PO_x signal for all aged samples. This indicates that the decrease in carbon signal is due to attenuation from a PO_x top layer, instead of the removal of carbon coating due to particle aging. While there is some formation of new PO_x species on the surface for all aged samples, for RP@C particles with the longest deposition time, only 2.0±0.9% of the elemental species in the analyzed region can be attributed to the PO_x species, compared to 24.8±3.7%PO_x for the uncoated sample. Analysis of the atomic percent composition indicates that longer carbon deposition times reduce the formation a PO_x top layer on the carbon coating, indicated by the larger attenuation of the carbon signal and an increase in PO_x signal in the P(2p) region for RP@C-short.

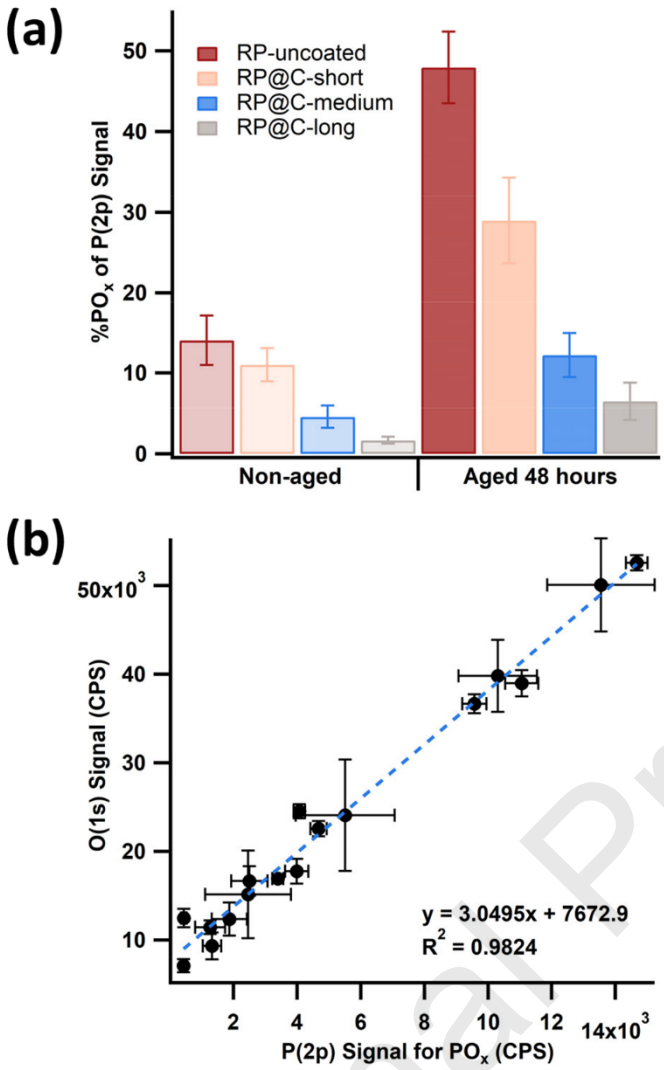

Figure 6. (a) Effect of aging and coating deposition time on area under the phosphate region of the P2p curve and (b) plot of integrated area for O(1s) vs. P(2p) phosphate region for all samples (nonaged and aged, uncoated and coated).

To first understand oxidation of the phosphorus surface, we quantified the percentage of P(2p) signal arising from oxidized phosphorus using equation 4. Using the adjusted area (SI equation 2), we normalize out any attenuation of the elemental phosphorus signal (130 eV) by the carbon coating. Figure 6a presents the impact of both aging and PDC deposition time on the POx composition measured using changes in the P(2p) region seen in Figure 5a. For non-aged samples, uncoated red phosphorus starts with more phosphate on the surface compared with samples that were carbon coated. As the deposition time increases, the initial phosphate on the surface decreases from 14±3% (RP-uncoated, non-aged) to 1.7±0.4% (RP@C-long, non-aged), indicating a level of protection that is only made more apparent after aging at 50°C for 48 hours. For uncoated aged RP, almost 50% of the phosphorus probed by XPS is oxidize phosphorus, while for RP@C-long, only 6.5±2.3% of the P(2p) region is attributed to oxidized species. All samples show a 3-4x increase in phosphate compared to non-aged. After aging in the IR cell, all samples show increased oxidized phosphorus on the surface, but PDC coated particles show suppression of the PO_x signal.

To understand the type of oxidized phosphorus on the surface of the particles, we investigated both the shifts in PO_x P(2p) binding energy and the ratio of O(1s) to PO_x P(2p) XPS intensities. As previously mentioned, after particles are aged, a distinct peak emerges at 134.2 eV (Figure

5a). This binding energy aligns with PO_3-containing compounds [33]. Additional confirmation of the phosphorus oxide species on the red phosphorus surface was provided by comparing the relationship of oxygen on the surface from the O(1s) region to the PO_x species on the surface from the P(2p) region. After taking the integrated area of O(1s) and the integrated area of the peak at ~134 eV of the P(2p) region, points for both non-aged and aged samples were graphed. Shown in Figure 6b, a slope of 3.04 was found, indicating the ratio of oxygen to phosphorus in PO_x form on the surface is 3:1, the ratio of phosphonate. XPS binding energy shifts in P(2p) region and oxygen-to-PO_x ratio indicates that the phosphorus oxide species is phosphonic acid and its derivatives.

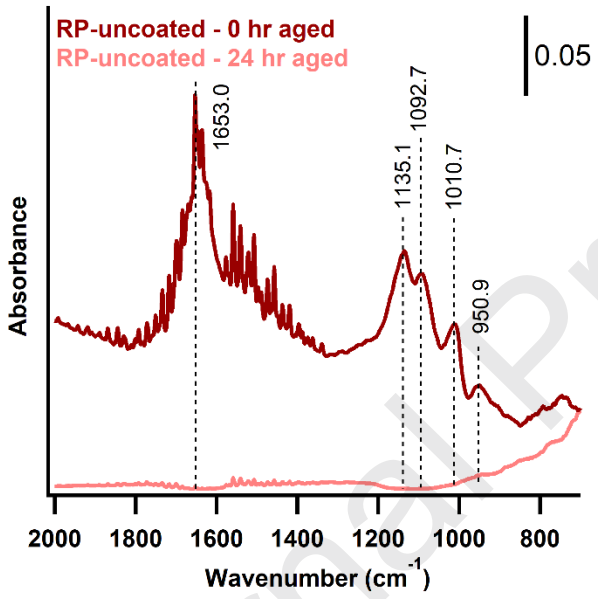

Figure 7. DRIFTS spectra of bare red phosphorus before and after aging in 100% humidity at 50°C.

Diffuse reflectance infrared spectroscopy was used to obtain a more comprehensive understanding of oxidized phosphorus species formed in situ during the aging process. Figure 7 shows IR spectra for uncoated red phosphorus suspended in zinc sulfide before and after aging for 24 hours. The non-aged sample does not show peaks in the phosphate region of the spectrum (below 1300 cm^{-1}). However, after aging at 50°C and 100% humidity, peaks grow in between 700-1200 cm^{-1} along with a strong peak at 1653 cm^{-1}, which can be attributed to OH deformation vibrations [34]. The peaks between 900-1200 cm^{-1} indicate the presence of both phosphoric acid (H_3PO_4) and phosphonic acid (H_3PO_3). The peak at 1135.1 cm^{-1} is attributed to P=O stretch for phosphonic acid in which an OH is replaced with an R group, likely P on the red phosphorus surface [35]. The peak at 1092.7 cm^{-1} is also attributed to a P=O stretch, but for that of phosphoric acid [35, 36]. The peak at 1010.7 cm^{-1} is also evidence for phosphoric acid on the surface, corresponding to the asymmetric P-O-(H) stretch for H_3PO_4 [37, 38]. Finally, the peak at 950.9 cm^{-1} signals a P-O-(H) stretch for phosphonic acid [37]. The DRIFTS spectrum of aged red phosphorus indicates the production of phosphoric acid and phosphonic acid on the surface.

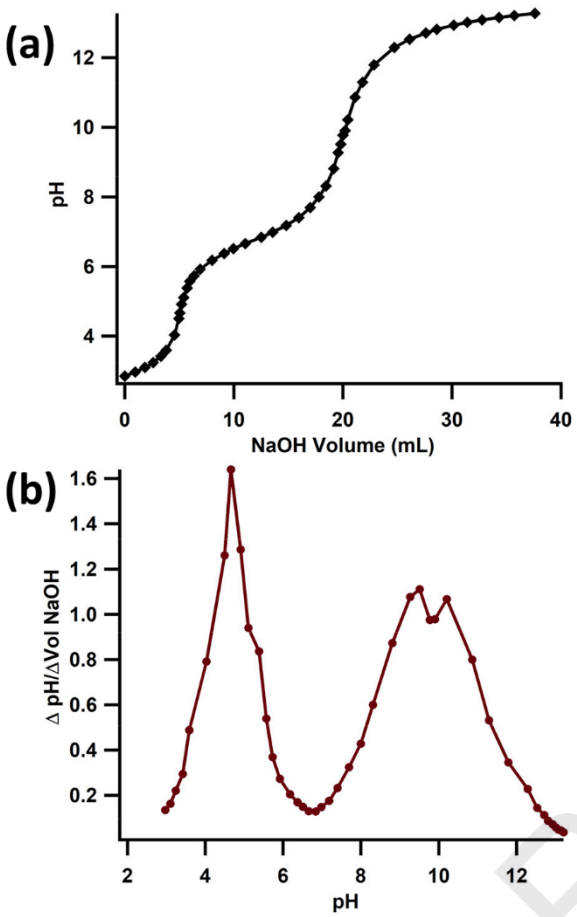

Figure 8. (a) titration curve of supernatant of bare, aged RP and (b) derivative of titration curve from (a).

While gas-phase IR can quantify the amount of PH_3 produced, we used acid-base titration to quantify the acid species that are also produced during the reaction. Figure 8a shows the titration curve obtained by extracting the supernatant from aged uncoated RP and titrating with NaOH, revealing two clear equivalence points. Taking the derivative of the titration curve (Figure 8b) more clearly shows two equivalence points near pH = 4.7 and pH = 9.5. Equivalence points for phosphoric acid at 25°C have previously been reported to occur at pH = 4.67 and pH = 9.79, while phosphonic acid shows a peak at pH = 4.89 [39]. Based on volumes from the titration, we calculated the solution contains 5.05×10^{-5} moles of H_3PO_4. From gas-phase IR, 1.78×10^{-5} mol of PH_3 was produced during the 48-hour aging process. Thus, our experiments imply formation of approximately 3 moles of H_3PO_4 for each mole of PH_3 produced under the conditions of our experiment. Identifying a specific mechanism for PH_3 degradation is challenging because oxidation can be induced by both O_2 and by H_2O in amounts that depend on experimental conditions. A previous study of red phosphorus degradation upon exposure to water and air [5] reported an overall approximate stoichiometry of:

$$3.5P_4 + 21H_2O + 11.275O_2 \rightarrow 5.2H_3PO_4 + 7.15H_3PO_3 + 0.65H_3PO_2 + PH_3$$

However, under oxygen-deficient conditions, a simpler stoichiometry can be identified:

$$2P_4 + 12\ H_2O \rightarrow 3H_3PO_4 + 5\ PH_3$$

Notably, the relative amounts of H_xPO_y species increases as the contribution from O_2 increases. Our data indicate a larger proportion of H_3PO_4 than could be produced by water alone. This in

turn suggests that under the conditions of our experiments, using a stagnant reservoir of water equilibrated with the atmosphere, both H_2O and O_2 are important in controlling the overall reaction. This conclusion is further supported by DRIFTS measurements showing the presence of phosphoric (H_3PO_4) and phosphonic (H_3PO_3) species on the surface. The presence of both species is consistent with prior studies using ion chromatography [5] and can be considered as a natural evolution of the surface starting with elemental P that is then successively oxidized to form surface -PO, -PO_2, and -PO_3 species prior to release into the aqueous medium as fully oxidized -PO_4 species, with appropriate levels of protonation. Notably, however, the effective thickness of the PO_3 layers measured by XPS can significantly exceed the thickness of a monolayer film; this shows that the formation of liquid H_3PO_4 and/or polyphosphate surface species is insufficient to halt further reactions of red phosphorus with water vapor and/or O_2. The kinetic data found from Figure 3 and presented in Table 1 show that the rate of reaction appears to decrease somewhat, suggesting that the liquid H_3PO_4 surface film reduces further reactions but does not halt them altogether.

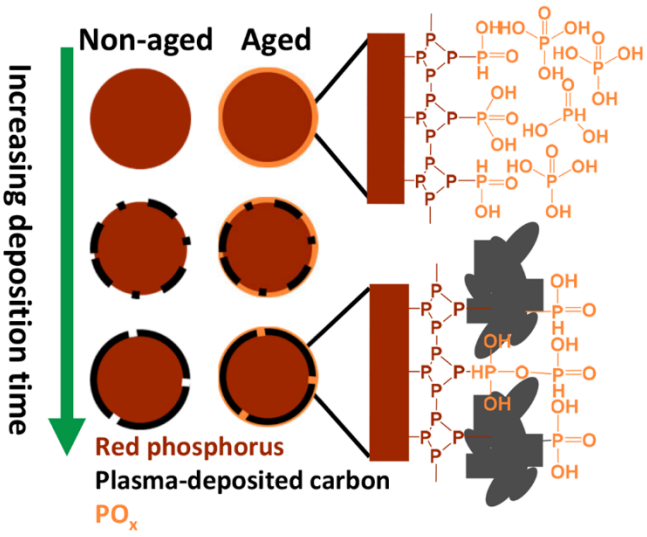

Figure 9. Proposed surface of red phosphorus after aging with and without plasma-deposited carbon protective coating. (*monolayer shown for simplification).

The influence of the carbon coating is summarized in Figure 9. Our FTIR data show that phosphine production is suppressed by the presence of a surface carbon coating. Using a longer plasma deposition time leads to particles with larger average carbon thicknesses (as measured by XPS) that are more resistant to reacting with water and oxygen to form PH_3. This increase in carbon coating thickness protects the red phosphorus from degradation, suppressing phosphine production (as measured by FTIR), and slowing the formation of a top layer of PO_x species that forms as the particles age (as measured by XPS). While very thin carbon films inhibit the reaction with water, the amount of surface -PO_x species observed from XPS is still larger than would be expected from a simple monolayer. While experiments cannot directly show a detailed mechanism of residual reactivity, we hypothesize that in the case of an imperfect coating with

small pinholes, reaction with water vapor at the pinholes produces liquid H_3PO_4 than can then spread beyond the pinhole, forming a thin layer extending across the entire particle surface. Longer deposition times have a higher probability of covering these pinholes, as seen in SEM images, reducing the exposed RP surface, leading to less measured phosphine and PO_x species.

4. Conclusion

We have demonstrated the efficacy of thin plasma-deposited carbon coatings of red phosphorus as a method of suppressing the production of toxic phosphine gas and acidic phosphorus-based byproducts. Using a combination of infrared spectroscopy and x-ray photoelectron spectroscopy, we quantified the production of phosphine, phosphoric acid, and phosphonic acid upon the exposure of red phosphorus to high humidity environments. XPS, diffuse reflectance IR, and titrations have provided data to construct a model of how plasma-deposited carbon is able to suppress phosphine and phosphoric-based acid generation (Figure 9). The plasma deposition method provides a thin, non-reactive carbon coating that provides a solution to long-term stability of red phosphorus regardless of the application.

5. Funding

National Science Foundation Grants CHE-2001611 and DMR-1720415

U.S. Army Contract W911SR19C0015.

6. CRediT author contributions

Paige C. Kinsley: Writing – Original Draft; Investigation; Methodology; Data curation; Visualization. **Aiping Zeng**: Resources; Methodology; Writing – Review & Editing. **Jenny K. Hedlund Orbeck**: Writing – Review & Editing. **Zachary B. Zander**: Conceptualization; Writing – Review & Editing. **Shaun Debow**: Conceptualization; Writing – Review & Editing. **Patrick J. Heaney**: Writing – Review & Editing; Conceptualization; Funding acquisition; Conceptualization; Supervision. **Robert J. Hamers**: Investigation; Methodology; Writing – Review & Editing; Supervision; Funding acquisition

7. Acknowledgements

This work was supported by the National Science Foundation under Grant No. CHE-2001611, the NSF Center for Sustainable Nanotechnology. The CSN is part of the Centers for Chemical

Innovation Program. Initial investigations of gas-phase PH_3 production were performed under the UW-Madison/US Army Combat Capabilities Development Command Chemical Biological Cooperative Research and Development Agreement #2046C and funded by the US Army under contract W911SR19C0015. Shared-facilities use of the x-ray photoelectron spectrometer and Raman spectrometer were supported by NSF through the University of Wisconsin Materials Research Science and Engineering Center (DMR-1720415).

Appendix A. Supplementary material

References

[1] N. Davies, Red Phosphorus for Use in Screening Smoke Compositions, in, Royal Military College of Science Shrivenham (United Kingdom), 1999.
[2] Y.H. Liu, Q.Z. Liu, C. Jian, D.Z. Cui, M.R. Chen, Z. Li, T. Li, T. Nilges, K. He, Z. Jia, C.W. Zhou, Red-phosphorus-impregnated carbon nanofibers for sodium-ion batteries and liquefaction of red phosphorus, Nat Commun, 11 (2020) 2520.
[3] M.R. Somayajulu, G.K. Gautam, A.S. Rao, Stabilisation of red phosphorus to prevent moisture absorption and suppression of phosphine release, Defence Sci J, 57 (2007) 817-824.
[4] United Nations Environment Programme., International Labour Organisation., World Health Organization., International Program on Chemical Safety., Phosphine and selected metal phosphides, World Health Organization; WHO Publications Center USA distributor, Albany, N.Y., 1988.
[5] V.J. Norris, Investigation of the Mechanism of the Oxidation of Red Phosphorus, in: Proceedings of the 27th International Pyrotechnics Seminar, IPSUSA, Inc., Grand Junction, CO, USA, 2000, pp. 207-216.
[6] C. Wilharm, F.E. Montgomery, M819 Red Phosphorus Smoke Reformulation Study, in: Proceedings of the 31st International Pyrotechnics Seminar, IPSUSA, Inc., 2004, pp. 11-16.
[7] J.A. Conner, J.A. Davenport, M819 Corrosion Study, in: Proceedings of the 27th International Pyrotechnics Seminar, IPSUSA, Inc, 2000, pp. 435-444.
[8] A.E. Cardell, T.T. Griffiths, T.A. Vine, Design Guide for Munitions Containing Red Phosphorus, in: Proceedings of the 31st International Pyrotechnics Seminar, IPSUSA, Inc., Ft. Collins, CO, USA, 2004.
[9] H. Staendeke, F.-J. Dany, J. Kandler, W. Klose, Stabilized red phosphorus and process for making it, in: USPTO (Ed.), Hoechst Aktiengesellschaft, United States, 1977.
[10] W. Racky, H. Cherdron, Moulding composition of thermoplastic materials, in: USTPO (Ed.), Hoechst Aktiengesellschaft, United States, 1974.
[11] F. Eisenträger, Key Parameters for the Stability of Red Phosphorus, in: Proceedings of the 31st International Pyrotechnics Seminar, IPSUSA, Inc., Fort Collins, CO, USA, 2004.
[12] J. Robertson, Properties of diamond-like carbon, Surface and Coatings Technology, 50 (1992) 185-203.
[13] H.Q. Li, H.S. Zhou, Enhancing the performances of Li-ion batteries by carbon-coating: present and future, Chem Commun, 48 (2012) 1201-1217.

[14] Q. Cao, H.P. Zhang, G.J. Wang, Q. Xia, Y.P. Wu, H.Q. Wu, A novel carbon-coated LiCoO2 as cathode material for lithium ion battery, Electrochemistry Communications, 9 (2007) 1228-1232.
[15] R. Saroha, A.K. Panwar, Effect of in situ pyrolysis of acetylene (C2H2) gas as a carbon source on the electrochemical performance of LiFePO4 for rechargeable lithium-ion batteries, Journal of Physics D: Applied Physics, 50 (2017) 255501
.
[16] M.L. Marcinek, J.W. Wilcox, M.M. Doeff, R.M. Kostecki, Microwave Plasma Chemical Vapor Deposition of Carbon Coatings on LiNi[sub 1⁄3]Co[sub 1⁄3]Mn[sub 1⁄3]O[sub 2] for Li-Ion Battery Composite Cathodes, Journal of The Electrochemical Society, 156 (2009) A48.
[17] M. Noborisaka, T. Hirako, A. Shirakura, T. Watanabe, M. Morikawa, M. Seki, T. Suzuki, Synthesis of Diamond-Like Carbon Films on Planar and Non-Planar Geometries by the Atmospheric Pressure Plasma Chemical Vapor Deposition Method, Japanese Journal of Applied Physics, 51 (2012) 090117.
[18] J.H.J. Scott, S.A. Majetich, Z. Turgut, M.E. McHenry, M. Boulos, Carbon Coated Nanoparticle Composites Synthesized in an RF Plasma Torch, MRS Proceedings, 457 (1996) 219.
[19] J.R. Conrad, J.L. Radtke, R.A. Dodd, F.J. Worzala, N.C. Tran, Plasma source ion-implantation technique for surface modification of materials, Journal of Applied Physics, 62 (1987) 4591-4596.
[20] S. Miyagawa, S. Nakao, M. Ikeyama, Y. Miyagawa, Deposition of diamond-like carbon films using plasma based ion implantation with bipolar pulses, Surface and Coatings Technology, 156 (2002) 322-327.
[21] D.A. Shirley, High-resolution X-ray photoemission spectrum of valence bands of gold, Physical Review B, 5 (1972) 4709.
[22] T.L. Barr, S. Seal, Nature of the use of adventitious carbon as a binding-energy standard, J. Vac. Sci. Technol. A-Vac. Surf. Films, 13 (1995) 1239-1246.
[23] R.A. Franking, E.C. Landis, R.J. Hamers, Highly stable molecular layers on nanocrystalline anatase TiO2 through photochemical grafting, Langmuir, 25 (2009) 10676-10684.
[24] D.P. Monaghan, K.C. Laing, P.A. Logan, P. Teer, D. Teer, How to Deposit DLC Successfully, Materials World, 1 (1993) 347-349.
[25] C.J. Powell, A. Jablonski, NIST Electron Effective-Attenuation-Length Database Version 1.3, in, National Institute of Standards and Technology, Gaithersburg, MD, 2011.
[26] P.J. Cumpson, The Thickogram: a method for easy film thickness measurement in XPS, Surf. Interface Anal., 29 (2000) 403-406.
[27] J.R. Durig, J.M. Casper, On the vibrational spectra and structure of red phosphorus, Journal of Molecular Structure, 5 (1970) 351-358.
[28] A.C. Ferrari, Raman spectroscopy of graphene and graphite: Disorder, electron-phonon coupling, doping and nonadiabatic effects, Solid State Commun, 143 (2007) 47-57.
[29] A.C. Ferrari, J. Robertson, Raman spectroscopy of amorphous, nanostructured, diamond-like carbon, and nanodiamond, Philosophical Transactions of the Royal Society A, 362 (2004) 2477-2512.
[30] L.R. Brown, R.L. Sams, I. Kleiner, C. Cottaz, L. Sagui, Line Intensities of the Phosphine Dyad at 10 μm, Journal of Molecular Spectroscopy, 215 (2002) 178-203.
[31] C. Sousa-Silva, A.F. Al-Refaie, J. Tennyson, S.N. Yurchenko, ExoMol line lists - VII. The rotation-vibration spectrum of phosphine up to 1500 K, Mon. Not. Roy. Astron. Soc., 446 (2015) 2337-2347.
[32] B. Lesiak, L. Kövér, J. Tóth, J. Zemek, P. Jiricek, A. Kromka, N. Rangam, C sp2/sp3 hybridisations in carbon nanomaterials–XPS and (X) AES study, Applied Surface Science, 452 (2018) 223-231.
[33] C. Wagner, A. Naumkin, A. Kraut-Vass, J. Allison, C. Powell, J. Rumble Jr, NIST X-ray Photoelectron Spectroscopy Database, NIST standard reference database 20, Version 3.4 (Web version), National Institute of Standards and Technology: Gaithersburg, MD, 20899 (2003).
[34] G. Socrates, Infrared and Raman Characteristic Group Frequencies: Tables and Charts, 3rd ed., Wiley, 2004.

[35] L.C. Thomas, R.A. Chittenden, Characteristic infrared absorption frequencies of organophosphorus compounds—I The phosphoryl (P=O) group, Spectrochimica Acta, 20 (1964) 467-487.
[36] W.W. Rudolph, Raman-and infrared-spectroscopic investigations of dilute aqueous phosphoric acid solutions, Dalton Transactions, 39 (2010) 9642-9653.
[37] L.C. Thomas, R.A. Chittenden, Characteristic infrared absorption frequencies of organophosphorus compounds—II. P-O-(X) bonds, Spectrochimica Acta, 20 (1964) 489-502.
[38] W. Jastrzbski, M. Sitarz, M. Rokita, K. Bułat, Infrared spectroscopy of different phosphates structures, Spectrochimica Acta Part A: Molecular and Biomolecular Spectroscopy, 79 (2011) 722-727.
[39] D.C. Harris, Quantitative chemical analysis, 8th ed., W.H. Freeman and Company, 2010.

Paige C. Kinsley: Writing – Original Draft; Investigation; Methodology; Data curation; Visualization. **Aiping Zeng**: Resources; Methodology; Writing – Review & Editing. **Jenny K. Hedlund Orbeck**: Writing – Review & Editing. **Zachary B. Zander**: Conceptualization; Writing – Review & Editing. **Shaun Debow**: Conceptualization; Writing – Review & Editing. **Patrick J. Heaney**: Writing – Review & Editing; Conceptualization; Funding acquisition; Conceptualization; Supervision. **Robert J. Hamers**: Investigation; Methodology; Writing – Review & Editing; Supervision; Funding acquisition

Declaration of interests

☒ The authors declare that they have no known competing financial interests or personal relationships that could have appeared to influence the work reported in this paper.

☐ The authors declare the following financial interests/personal relationships which may be considered as potential competing interests:

Highlights

- Plasma-deposited carbon coating provides thin, non-reactive surface on red phosphorus
- Carbon coating suppresses toxic byproducts from red phosphorus break down by H_2O and O_2
- XPS and IR data elucidate mechanism of PH_3 and PO_x production by carbon coating
- Carbon coating provides stability of red phosphorus in humid, ambient environments